https://doi.org/10.48048/tis.2022.6178

Characteristic Making of $Ba_{0.4}Sr_{0.6}TiO_3$ Thin Film Nanoparticles

Rahmi Dewi[1,*], Krisman[1], Zuhdi[2], Ari Sulistyo Rini[1] and Tengkusaidluqman Hussains[1]

[1]Department of Physics, Math and Science Faculty, Universitas Riau, Pekanbaru 28293, Indonesia
[2]Faculty of Teacher Training and Education, Universitas Riau, Pekanbaru 28293, Indonesia

([*]Corresponding author's e-mail: drahmi2002@yahoo.com)

Received: 28 December 2020, Revised: 8 May 2021, Accepted: 15 May 2021

Abstract

Presently, the research on thin films is essentially useful in the world of science and technology. Therefore, this study aims to explore Barium Strontium Titanate (BST) as the basis in the making of dynamic random access memory (DRAM). This DRAM technology produces small cells that have faster operations, lower energy, longer data storage period, and are found to havemade up of Barium Strontium Titanate nanoparticles ($Ba_{0.4}Sr_{0.6}TiO_3$; BST). BST applications in the form of capacitors can be used as gas sensors, temperature sensors, microwave phase shifters, tunable filters, oscillators, infrared sensors, etc.

The main component of BST was showed by the sol-gel method, and the device structure constituted of $Si/SiO_2/RuO_2/TiO_2$ /$Ba_{0.4}Sr_{0.6}TiO_3$/Al. All the samples were annealed at 400, 450, 500, 550, 600, 650 and 700 ℃ for 60 min. The sample was annealed to see the crystalline structure of the sample.

The sol gel method was chosen in the process of making thin films of $Ba_{0.4}Sr_{0.6}TiO_3$ (BST) because this method was easier and cheaper than other techniques. The thin film was characterized by optical and electrical properties. The results showed that a rise in the annealing temperature increased the crystalline, grain size, thickness and surface roughness of the sample. The characterization was carried out on the device structure ($Si/SiO_2/RuO_2/TiO_2/Ba_{0.4}Sr_{0.6}TiO_3$/Al) in order to examine the optical and electrical properties, including the current density and the dielectric features. At the annealing temperature of 700 ℃, the device showed the best value, with the absorption peak at the wavelength of 688 nm. And also, with the dielectric constant (ε_r) of 2,500, capacitance (C) of 22.10 nF, dense alternating current (ρ_{au}) of 2.54×10^4 Ω.m, conductance (σ_{au}) of 1.20×10^{-2} 1/Ω.m, and current density of 9.85×10^{-5} A.cm^{-2} at 0.5 V. The results of characterization of this capacitor are very good to be used as an infrared sensor.

Keywords: BST Nanoparticles, Sol-gel method, Annealing temperature, Electrical properties, Dielectric properties

Introduction

Presently, the study on thin films is found to be essentially useful in world of science and technology and has started more than one hundred years ago [1]. The rapid advances in the computer fields, such as high-tech products, those with massive capacities, and the competition from mini device manufacturers, have demanded the production of nano-sized electronic components. This is in line with developments and advances in the production of semiconductor devices, such as transistors, capacitors, diodes, and an integrated circuit [2].

The nature of thin films differs from the state of materials that makes up their shapes and is characterized by the optical and electrical properties [3]. The commonly studied optical properties are transmission and absorption. Furthermore, a thin film layer of conductors usually has high ability to transmit visible and reverse infrared light. Besides having good optical properties, it also possesses electrical resistance, which is low enough to make it a good electricity conductor. Therefore, by having both good optical and electrical properties, the use of thin films becomes very broad, encapsulating in various fields of energy, electronics, optoelectronics, etc. Thin film applications such as gas sensors are electro-chemical sensors, which are devices that can respond to changes in the chemical environment around them by generating electrical signals [4-6]. In terms of general applications, thin films have reached various fields of science. In the construction sectors, especially those related to metal materials, thin layers are used as a material to increase corrosion resistance [7]. In the field of electronics, thin films are used to

make capacitors, semiconductors, and sensors [8]. In the field of decoration, thin layers are used to create a more attractive appearance and are used in home decor, jewelry, and other accessories.

This research aims to explore the thin film of barium strontium titanate (BST). The perovskite materials with high dielectric constants, such as Barium Strontium Titanate (BST), plumbum zirconium titanate (PZT), and strontium titanate ($SrTiO_3$), are recommended as the basis for making dynamic random access memory (DRAM) [1]. This DRAM technology produces small cells that have faster operations, lower energy, and longer data storage period [9]. The materials that meet these characteristics and conditions are highly needed, with a very suitable one being the BST [10].

Barium titanate ($BaTiO_3$) is an important base structure used as a ferroelectric ceramic material, and strontium titanate ($SrTiO_3$) also a paraelectric feature. Barium Strontium Titanate (BST) is an important ferroelectric ceramic structure used extensively as a dielectric material. The BST has high dielectric constant and low electricity leakage [11]. The mixture of both $BaTiO_3$ and $SrTiO_3$ causes changes to the Curie temperature [Tc], i.e. from the ferroelectric transition to paraelectric material. BST reduces from 120 ℃ to room temperature [12], which is a linear Tc reduction by 3.4 ℃ per mole of strontium. Therefore, 0.3 mole of strontium decreases Tc to room temperature [4].

When sunlight hits the surface of a thin film, not do all rays penetrate. Some of the lights are reflected, as well as scattered. Furthermore, light absorption also applies. Therefore, the optical properties contained in thin films are the reflection, transmission, and polarization of light for wavelengths that affect the normal angle, namely from 300 - 800 nm [13].

The technique used to determine the electrical characteristics of a dielectric material is complex impedance method. This technique uses alternating cues in the form of sinusoid, which is the output signaling through a linear system, which has the same frequency as the input signal. Impedance modulus, $|Z|$ and the phase angle, (Φ), are determined when output signal in form of a sine is compared to that of the input [14].

In general, the polycrystalline ceramic impedance spectrum consists of 3 perfect half-rounded curves that represent electrical properties of the sample as shown in **Figure 1**. The impedance spectrum of complex numbers shows the main components in a material such as the grains, grain boundaries, and interface sample or electrodes. When a current flows through positively and negatively, the electrode ends up not polished then functions as a capacitor with unidirectional resistance. Impedance value is a combination of 2 components, namely the real (Z'), and imaginary components (Z'') [15].

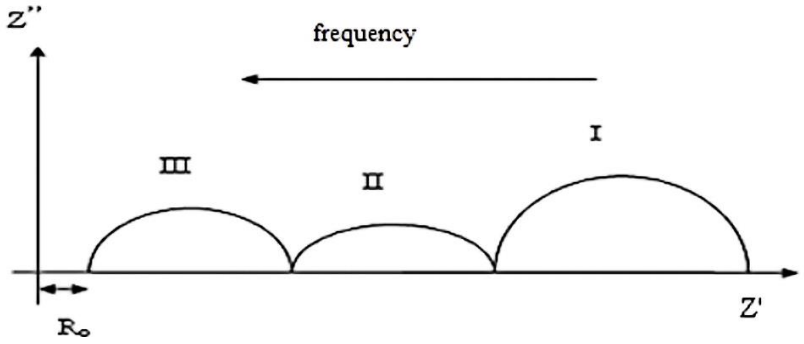

Figure 1 Impedance spectrum for polycrystalline samples.

Curve I represents the process that applies between interface of electrode or electrolyte at low frequencies (< 10 kHz), while curve II represents the process that applies to grain boundaries at mid frequencies (1 - 100 kHz). Curve III, which applies to frequencies (> 10 kHz), is the curve that represents sample solid process. An equivalent circuit that can describe perfect impedance spectrum for the 3 processes above is shown in **Figure 2** [15].

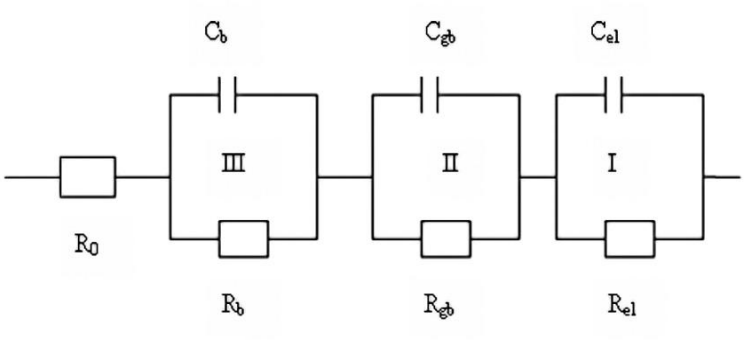

Figure 2 Equivalent circuit to describe curves I, II and III.

R_0 represents leap of a complex impedance spectrum to that of the right. This is because the starting point for each complex impedance spectrum is not actually the coordinates (0.0), yet shifts slightly to the real one's right [16].

The measurement of complex impedance, i.e. The real, Z and imaginary impedance, Z. Dielectric constant (ε_r'), conductance (σ), capacitance (C), and alternating current density (ρ_{au}) is calculated using complex impedance values (Z^*) obtained from measurements [17].

$$Z^* = Z' - jZ'' \tag{1}$$

with $j = (-1)^{1/2}$

Complex capacitance value (C^*) at a certain frequency is obtained through the relationship of:

$$C^* = \frac{1}{j\omega Z^*} \tag{2}$$

where ω = angular frequency = $2\pi f$

Taking into account the thickness d and surface area A, the complex resistance (ρ^*) is written as:

$$\rho^* = \rho' - j\rho'' \tag{3}$$

Complex conductance (σ^*) expressed as :

$$\sigma^* = \frac{1}{\rho^*} = \sigma' + j\sigma'' \tag{4}$$

Dielectric constant value (ε_r') is calculated using the equation:

$$\varepsilon_r' = \frac{C^*.d}{\varepsilon_0.A} \tag{5}$$

where, d equals the thickness of the film, C^* complex capacitance in units of farads. ϵ_o vacuum constant (8.85×10^{-12} F/m), and A surface area of upper electrode film in units of m^2 [16].

Materials and methods

The process of making thin films of $Ba_{0.4}Sr_{0.6}TiO_3$ (BST) by using sol-gel is because the method is easier and cheaper than other techniques. The basic ingredients are Barium acetate Ba powder ($C_4H_6O_4$), strontium acetate ($Sr(CH_3CO_2)_4$, and titanium (IV) Isopropoxide liquid $(Ti(OCHCH)_3)_2)_4$ isused in making BST thin films.

Before the process of solution making is carried out, silicon substrate (Si) type-p boron which has a single oriented crystal (100), and a thickness of 625 μm with resistance 14 - 22 Ω cm, gets cleaned first. The SiO_2 layer (150 nm) was coated over Si substrate by e-gun method, with vacuum condition 2.5×10^{-5} mbar. Furthermore, ruthenium oxide layer RuO_2 (100 nm) was coated over Si/SiO_2 substrate, with the sputtering method. RuO_2 as a positive electrode was then annealed into the air for 30 min, at 500 ℃. After being coated with RuO_2 film, 70 nm thick titanium oxide coating, [TiO_2] is superimposed on $Si/SiO_2/RuO_2$ substrate using the e-gun method, then annealed for 30 min at a 500 ℃ temperature. The purpose of this annealing process is to produce a stable film. The TiO_2 coating serves as a barrier to block injection of currents between the substrate and ferroelectric films [18]. The $Si/SiO_2/RuO_2/TiO_2$ substrates annealed are then coated with BST material using the sol-gel method. Furthermore, negative electrode i.e. Aluminum, Al 100 nm thick, is coated by using the e-gun method. Flow chart of the process of making BST thin films by the sol-gel method is shown in **Figure 3**.

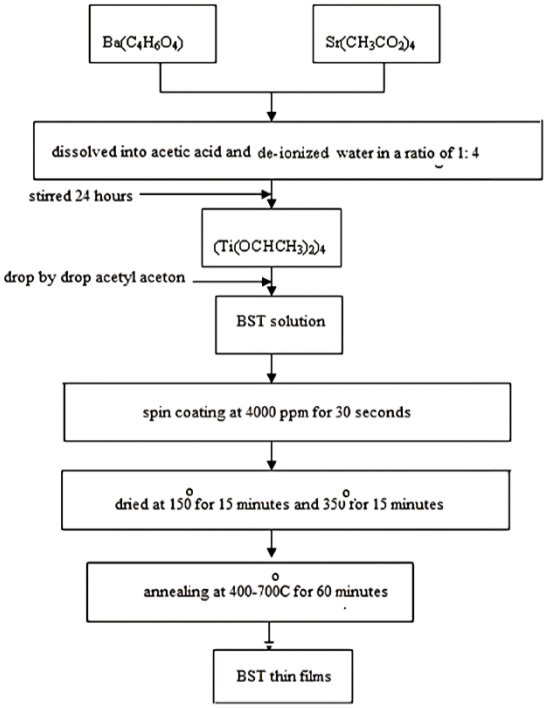

Figure 3 Flowchart of the process of BST thin films making.

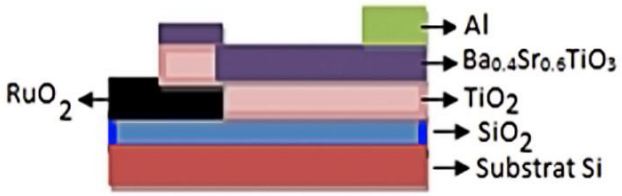

Figure 4 Device structure of a thin film of $Ba_{0.4}Sr_{0.6}TiO_3$.

A device with a structure of Si /SiO_2 /RuO_2 /TiO_2 /$Ba_{0.4}Sr_{0.6}TiO_3$ /Al as shown in **Figure 4** above.

Results and discussion

This section discusses results obtained from the basic characterization of thin films such as microstructure properties of the materials, morphology, grain size, thickness, optical features, and components of BST devices such as electrical and current densities, complex impedances, dielectric exhibition, with annealing temperature variations.

X-ray diffraction (XRD) characterization

XRD spectrum of film, $Ba_{0.4}Sr_{0.6}TiO_3$, is being annealed at 350 ℃ temperature before and 400 ℃ to 700 ℃ after. **Figure 5** shows the XRD spectrum before being annealed at 350 ℃ and after at 400 - 700 ℃. It is obtained that the film without and after being annealed at temperatures of 400, 450, 500 and 550 ℃ has an amorphous structure, while at 600, 650 and 700 ℃, is crystalline. Crystalline film, $Ba_{0.4}Sr_{0.6}TiO_3$, starts at 600 ℃ and above. The peak of the BST phase starts at 600 ℃, and crystalline increases to 700°C temperature. Therefore, this explains that $Ba_{0.4}Sr_{0.6}TiO_3$ crystalline levels increase along with high annealing temperature.

Low annealing temperature below 600 ℃ causes thin film to not undergo crystalline process. According to Pandey *et al.* (2019), at low temperatures, it does not have sufficient power to overcome basic energy between the perovskite (the phase of ferroelectric structure becomes paraelectric) and the mid-metastable phase (the phase between the ferroelectric structure and the paraelectric). The results of this study are the same as those reported by Zhou *et al.* [12]; Guo *et al.* [19]; Tarnaoui *et al.* [20]; Everhardt *et al.* [21]; and Wang *et al.* [22]. Therefore, this is then explained by the increase in annealing temperature, which causes the atom to have enough energy to move, so that crystalline is also increasing [23].

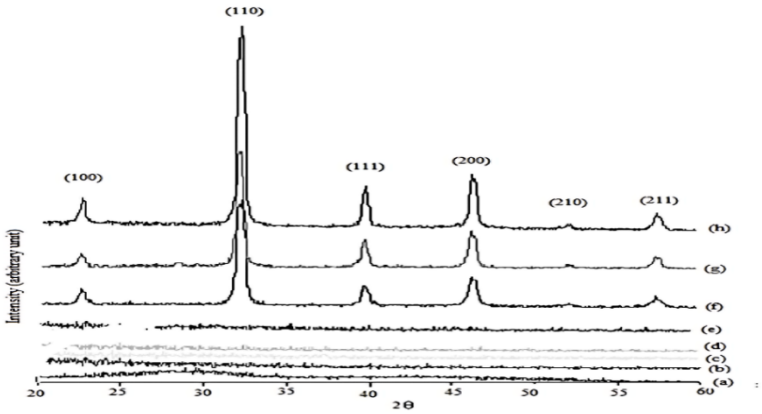

Figure 5 XRD spectrum of Si/SiO_2/ substrate $Ba_{0.4}Sr_{0.6}TiO_3$ before being annealed (a) at the temperature of 350 ℃ and after being annealed (b) 400, (c) 450, (d) 500, (e) 550, (f) 600, (g) 650 and (h) 700 ℃.

Atomic force microscopy (AFM) characterization

Figure 6 shows a 3-dimensional surface morphology image structure of a thin film, $Ba_{0.4}Sr_{0.6}TiO_3$. (a) without and after being annealed, (b) 600, (c) 650, and (d) 700 ℃. Before the film morphology got annealed, the surface had been found to be rather slippery and flatter than it became thereafter. Hilly morphology was found to be increasing with high annealing temperature. A smooth and flat film surface is an important producing quality device feature, with surface roughness smaller than 100 nm.

Table 1 Surface roughness values $Ba_{0.4}Sr_{0.6}TiO_3$ with different annealing temperatures.

Annealing temperature (℃)	Surface roughness Ra (± 0.01 nm)
Without annealing	8.53
600	11.35
650	18.40
700	42.00

The image of the film surface morphology provided by the sol-gel method has also been investigated by Huang *et al.* (2017) through heating the substrate at 750 ℃ temperature for 1 h [24]. The results of their study found that the average surface roughness of $Ba_{0.4}Sr_{0.6}TiO_3$film increased with the increasing annealing temperature, i.e., 3.8 and 7 nm, respectively. This was also investigated by Zhao *et al.* [25]; Gautam *et al.* [26] which shows that BST films annealed at an increasing temperature had high average surface roughness. This sharp increase in roughness can be attributed to grain growth due to increased annealing temperature. When a BST thin film is exposed to an electric field, it is generally assumed that there is a higher electric field density at the crest of a sharp valley than on a smoother surface. Therefore, grain growth can have a negative effect and lead to an increase in leakage currents [27].

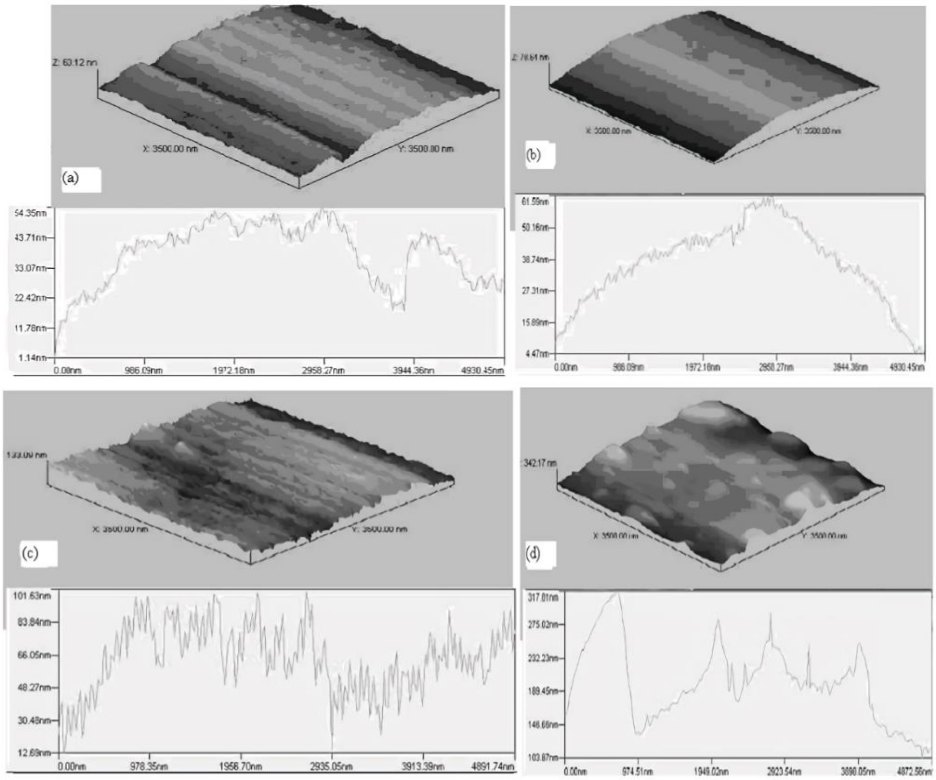

Figure 6 3-dimensional image of the surface morphological structure of a thin film $Ba_{0.4}Sr_{0.6}TiO_3$ at (a) without being annealed and after being annealed at (b) 600, (c) 650, and (d) 700 ℃.

Scanning electron microscopy (SEM) characterization

Figure 7(a) shows a thin film of $Ba_{0.4}Sr_{0.6}TiO_3$ without being annealed, then carried out at 400 ℃, indicating that the film structure has no grain or rather invisible. For films scaled at temperatures of 450 to 550 ℃, result showed that grains were initially visible, with their distance so far in size between 80 and 150 nm. Thin film, $Ba_{0.4}Sr_{0.6}TiO_3$, annealed at the temperature 600 to 700 ℃, showed the grain sizes of 47.5, 51.1, and 53.5 nm, respectively. The grain sizes increased with appearance of dense fine ones, without any distance in between. The larger grain size is due to the increase in annealing temperature. Zaman *et al.* [4] also reported the same result that the more increase in annealing temperature, the larger the grain size. According to Manogowri (2016), with the increasing annealing temperature, movement of atoms may rise up as well [28]. Atomic movement is the ability of atoms to move from one state to another in a crystallized or non-crystallized material; besides, it encourages atomic surface locomotion that causes small droplets to combine and form larger ones. This prevailing event is more recognized as a grain growth. Grain growth is a process in which free or nearly free average size grains increase regularly at a high temperature, without changes in the sprinkling process. The same research results have also been reported by Zhang *et al.* [29]; Wang *et al.* [30]; Chen *et al.* [31]; Lee *et al.* [32].

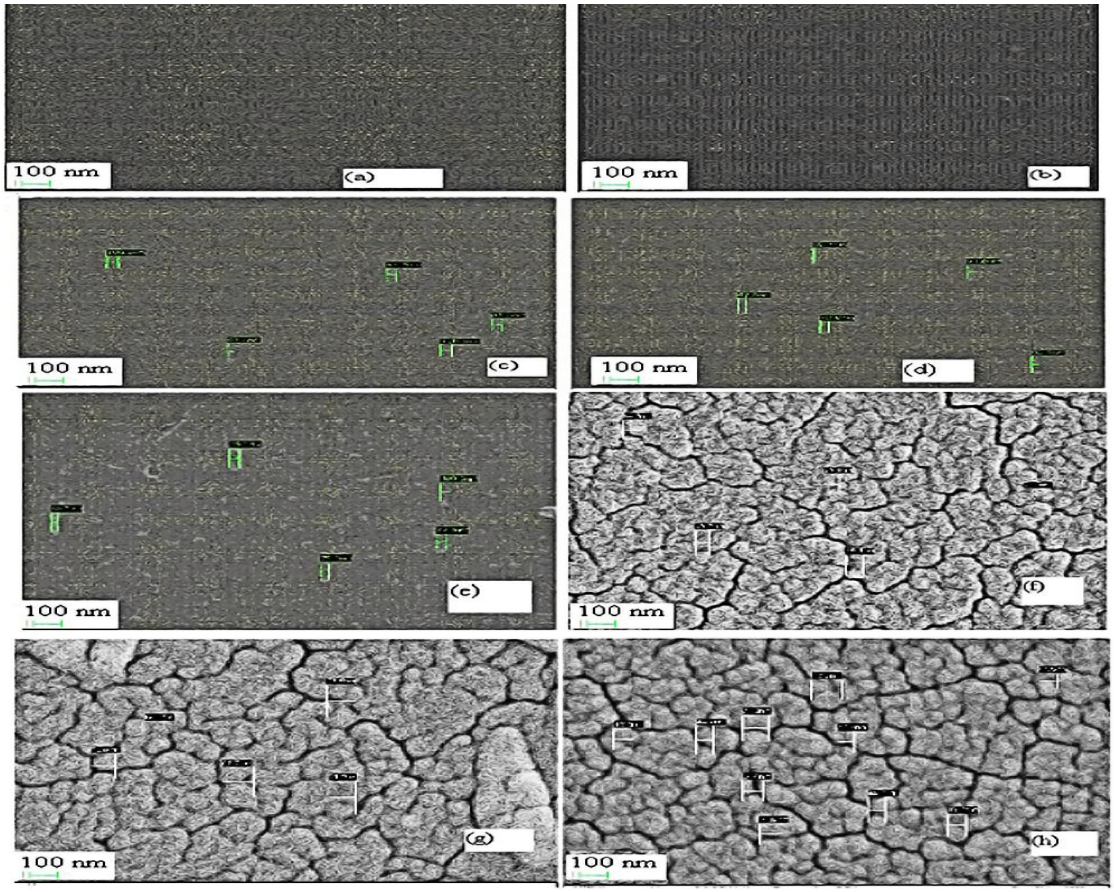

Figure 7 SEM micrographs for thin films $Ba_{0.4}Sr_{0.6}TiO_3$, (a) after being supplied, after being annealed at the temperature (b) of 400 °C, (c) 450 °C, (d) 500 °C, (e) 550 °C, (f) 600 °C, (g) 650 °C and (h) 700 °C.

From the measurement of thin film thickness by using SEM, values have been obtained as shown in **Table 2**. In **Table 2**, the annealing temperature of 400 to 550 °C occurs abnormalities in the thickness of the film, which is because the film is in an amorphous state, crystalline BST appears at annealing temperatures of 600, 650, and 700 °C which have a regular atomic structure, so that the thickness of the film increases regularly with increasing annealing temperature.

Table 2 BST film thickness and average film grain size.

Temperature (°C)	**Film thickness (± 0.1 nm)**	**Average grain size (± 0.1 nm)**
After provided	312.6	No details
400	508.0	No details
450	1541.0	80.0
500	2077.0	100.0
550	692.2	150.0
600	217.7	47.5
650	245.6	51.1
700	438.2	53.5

BST thin film without annealing has a thickness of 312.6 nm and is annealed at 400 ℃ indicating a result of 508 nm. The thickness of the BST film increases after being annealed. The films annealed at temperature of 450 to 550 ℃ showed respective thickness: 1541, 2077, and 692.2 nm. The BST film thickness is irregular with increasing annealing temperature. For thin films of BST annealed at the temperature of 600 to 700 °C, it was found that the thickness skyrocketed with the increase of the annealing temperature, respectively i.e., 217.7, 245.6 and 438.2 nm. Therefore, the thickening of the thin film rises with increasing annealing temperature caused by differences in grain size. **Figure 8** shows the thickness value of the film and the average size of BST grain obtained with variations of the annealing temperature.

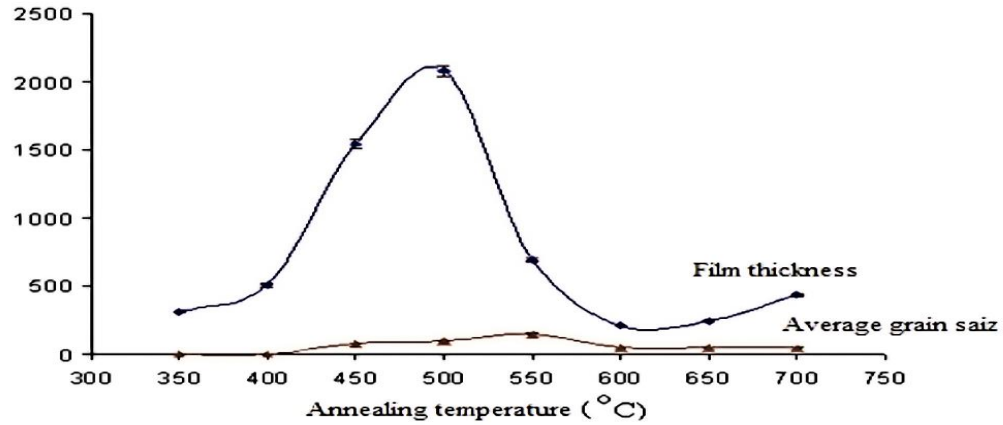

Figure 8 Relationship of temperature with BST film thickness and average grain size.

Optical characterization

Figure 9 showed the optical absorption constant value, α on BST films, with the annealing temperatures of 600, 650 and 700 ℃ coated over the quartz substrate surface. The plotted graphs showed that there was a peak in the same wavelength region at 688 nm.

It was noted that the absorption values increase with annealing temperature reduction. This is explained from the formula of the absorption coefficient (α) as a wave function, namely:

$$\alpha = \frac{2.303A}{t} \quad (6)$$

where a is the absorbance and t is the thickness of the film. From Eq. 6, it is known that increasing film thickness means increasing annealing temperature, so the absorption coefficient decreases [28].

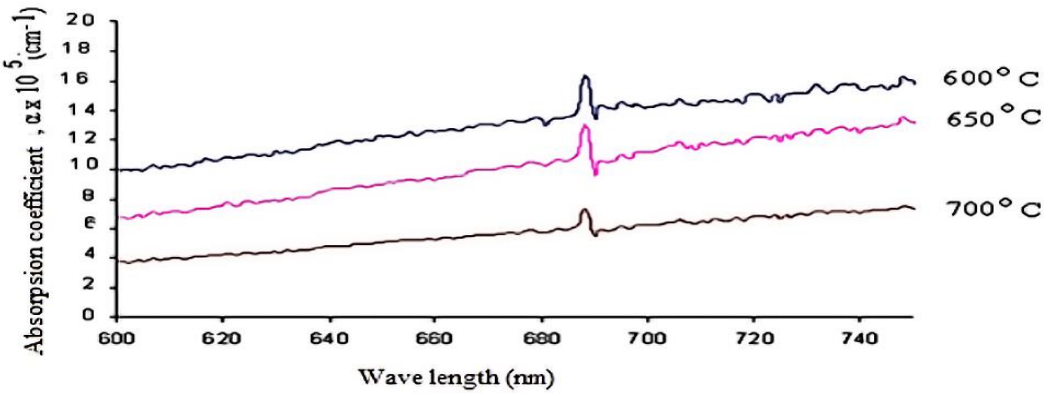

Figure 9 Complete absorption, α as a function of the wavelength of BST thin films at the annealing temperatures of 600, 650 and 700 °C.

Current and voltage characterization (I-V)

Figure 10 showed the I-V characterization of BST thin films, with annealing temperature variation of 600, 650 and 700 °C. The current density is 9.40×10^{-7}, 2.77×10^{-5} and 9.85×10^{-5}A.cm^{-2} at 600, 650 and 700 °C, respectively, at 0.5 V. This proved that the device with 650 and 700 °C is not good because electric current in the forward direction is flowing more slowly with the increasing voltage values. Besides, having a surface film which is not too slippery and flat compared to that of 600 °C. The device is said to have good properties when the electric current flowing in the forward direction rises rapidly with the increase in voltage value, while the skyrocket in the current to the uplift in the voltage value in the reverse direction is very small.

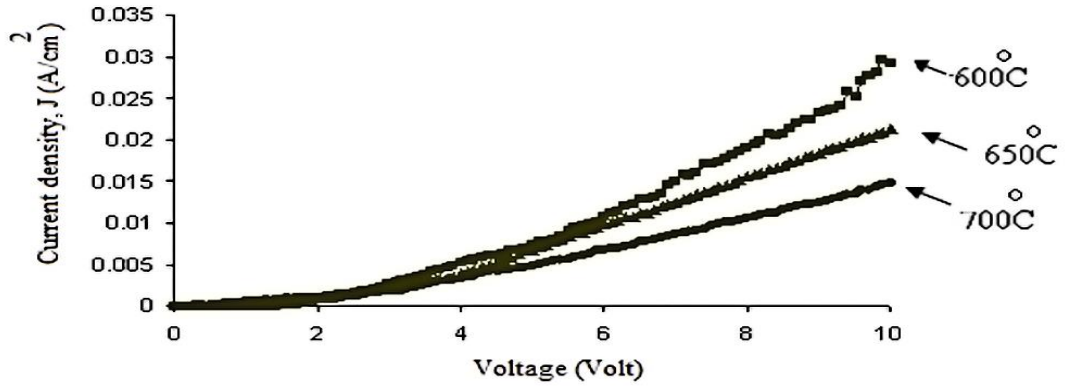

Figure 10 I-V Characterization of BST devices with varying annealing temperature of 600, 650 and 700 °C.

Characterization of spectroscopy

Impedance characterization is carried out using complex impedance spectroscopy, which is used to determine the properties of the grain components, boundaries, and nature of the sample interface with electrodes to the alternating current given. The frequency range used in this measurement is 10 Hz to 1 MHz. Measurement and calculation of data are obtained at 1 kHz Zhou *et al.* [12]; Veerapandiyan *et al.* [23]; Pandey *et al.* [33]; Zhai *et al.* [34] by using Eqs. (1) to (5). The 1 kHz is the best value to represent the dielectric properties of ferroelectric material. It was found that the device had a dielectric constant and a high resistance value at room temperature as shown in **Table 3**.

Table 3 Effect of annealing temperature on dielectric constant (ε_r), capacitance (C), alternating current density (ρ_{au}) and conductance (σ_{au}) at a frequency of 1 kHz.

Annealing temperature (°C)	Dielectric constant (ε_r)	Capacitance (C) nF	Alternating current dencity (ρ_{au}) Ω.m	Conductance (σ_{au}) 1/Ω.m
600	163	1.44	2.41×10^{7}	2.171×0^{-5}
650	779	6.89	1.06×10^{6}	5.10×10^{-4}
700	2,500	22.10	2.54×10^{4}	1.20×10^{-2}

The BST device has a high-density value, which is in the range of 10^4 to 10^7 Ω.m. The density value for a good dielectric material is between 10^{10} to 10^{12} Ω.m.

Figure 11, a to b, each showed a BST device with a dielectric constant value (ε_r') and dielectric loss (ε_r'') as a function of the frequency relating to the annealing temperature. Besides, the dielectric constant value (ε_r') and dielectric loss at 1 kHz are 2,500 and 30,000, respectively.

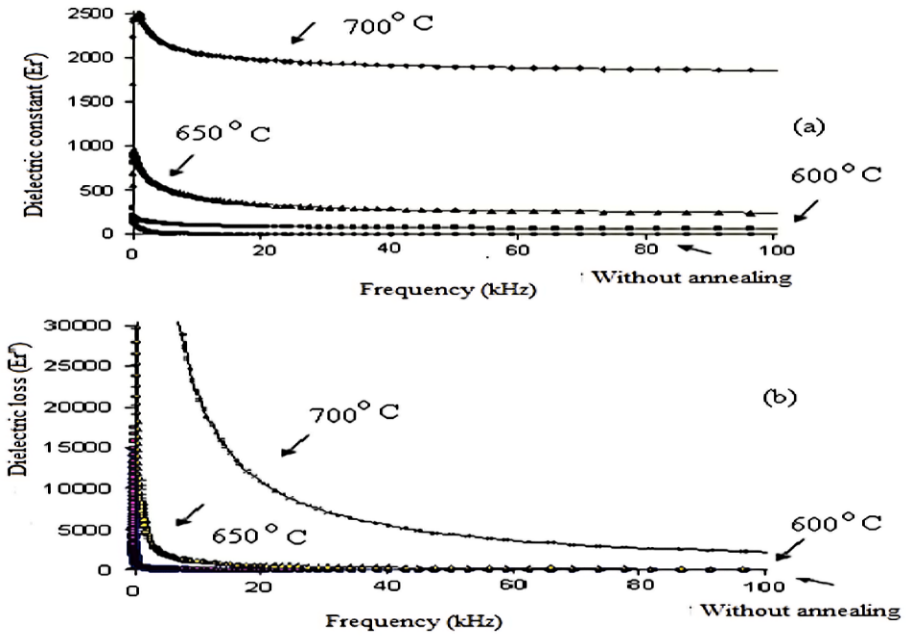

Figure 11 BST device with (a) Dielectric constant plot (ε_r'), (b) and Dielectric loss (ε_r'') to frequency (kHz) without and after annealing at 600, 650 and 700 °C.

Conclusions

The sol-gel method successfully showed the BST nanoparticles (Si/ SiO_2/ RuO_2/ TiO_2/ $Ba_{0.4}Sr_{0.6}TiO_3$ /Al) at 400 to 700 °C. The results of the XRD, AFM, SEM characterization, and their optical properties showed that BST material is included in the nanomaterial. The results of I-V characterization and impedance of the device showed the best value at 700 °C dielectric constant (ε_r) of 2,500, capacitance (C) of 22.10 nF, alternating current density (ρ_{au}) of 2.54×10^4 Ω.m, conductance (σ_{au}) of 1.20×10^{-2} 1/Ω.m, and the current density of 9.85×10^{-5} A.cm^{-2} at 0.5 V. Therefore, these findings are used as capacitors and basic material for making DRAM. Applications that use this BST material are infrared sensors, gas sensors, temperature sensors, pressure sensors, and others.

Acknowledgements

The authors are grateful to the Department of Physics, FMIPA, University of Riau, and the colleagues in the material laboratory, Department of Physics, Faculty of Mathematics and Natural Sciences, University of Riau, Indonesia.

References

[1] S Yu, W Lou, C Zhang, M Wu, L Ge, H Dong and L Li. Textured multilayers with enhanced tunable performance. *J. Alloys Comp.* 2018; **781**, 689-95.

[2] RA Malik, A Hussain, M Acosta, J Daniels, HS Han, MH Kim and JS Lee. Thermal-stability of electric field-induced strain and energy storage density in Nb-doped BNKT-ST piezoceramics. *J Eur. Ceram. Soc*. 2018; **38**, 2511-9.

[3] BI Edmondson, S Kwon, CH Lam, JE Ortmann, AA Demkov, MJ Kim and JG Ekerdt. Epitaxial, electro-optically active barium titanate thin films on silicon by chemical solution deposition. *J. Am. Ceram. Soc.* 2020; **103**, 1209-18.

[4] T Zaman, MK Islam, MA Rahman, A Hussain, MA Matin and MS Rahman. Mono and co-substitution of Sr^{2+} and Ca^{2+} on the structural, electrical and optical properties of barium titanate ceramics. *Ceram Int.* 2019; **45**, 10154-62.

[5] LA Patil, MD Shinde, AR Bari and VV Deo. Highly sensitive and quickly responding ultrasonically sprayed nanostructured SnO_2 thin films for hydrogen gas sensing. *Sensor Actuator B Chem.* 2009; **143**, 270-7.

[6] AZ Adamyan, ZN Adamyan and VM Aroutiounian. Study of sensitivity and response kinetics changes for SnO_2 thin-film hydrogen sensors. *Int. J. Hydrogen Energ*. 2009; **34**, 8438-43.

[7] S Saloum and B Alkhaled. Structural, optical and electrical properties of plasma deposited thin films from hexamethyldisilazane compound. *Acta Phys. Pol. A* 2011; **119**, 369-73.

[8] MM Liz, K Muller, L Heinke and HJ Osten. Integration of thin film of metal-organic frameworks in metal-insulator-semiconductor capacitor structures. *Microporous Mesoporous Mater.* 2018; **265**, 185-8.

[9] C Zhang, Z Ling, G Jian and FX Chen. Dielectric properties and point defect behavior of antimony oxide doped Ti deficient barium strontium titanate ceramics. *Trans. Nonferrous Met. Soc. China* 2017; **27**, 2656-62.

[10] B Liu, X Wang, R Zhang and L Li. Energy storage properties of ultra fine-grained $Ba_{0.4}Sr_{0.6}TiO_3$-based ceramics sintered at low temperature. *J. Alloys Comp.* 2017; **691**, 619-23.

[11] Z Zhao, X Song, T Zhang, K Hu, X Liang, S Li, Y Zhang, I Baturin and V Shur. Influence of lanthanum substitution on microstructure and impedance behavior of barium strontium titanate glass-ceramics. *J. Appl. Phys.* 2019; **126**, 074101.

[12] M Zhou, R Liang, Z Zhou and X Dong. Novel $BaTiO_3$-based lead-free ceramic capacitors featuring high energy storage density, high power density, and excellent stability. *J. Mater. Chem. C* 2018; **6**, 8528-37.

[13] V Kavitha, P Mahalingam, M Jeyanthinath and N Sethupathi. Optical and structural properties of tungsten-doped barium strontium titanate. *Mater. Today Proc.* 2020; **23**, 12-5.

[14] S Sahoo, S Hajra, M De and RNP Choudhary. Resistive, capacitive and conducting properties of $Bi_{0.5}Na_{0.5}TiO_3$-$BaTiO_3$ solid solution. *Ceram. Int.* 2018; **44**, 4719-26.

[15] T Akhtar and M Anis-ur-Rehman. Reduced impedance in dual substituted strontium cobaltite nanoparticles for renewable energy applications. *Mater. Res. Express* 2020; **7**, 015525.

[16] D Shreiber, W Zhou, G Dang, M Taysing-Lara, G Metcalfe, E Ngo, M Ivill, SG Hirsch and MWCole. Tunable metamaterial device for THz applications based on $BaSrTiO_3$ thin film. *Thin Solid Films* 2018; **660**, 282-6.

[17] JG Anderson. *Dielectrics*. Reinhold, New York, 1964, p. 1-171.

[18] S Suhailrashid, CO Sreekala and SK Menon. Dielectric resonator antenna on Ba TiO_3 embedded with TiO_2 nano composite for Wi-Fi applications. *IOP Conf. Ser. Mater. Sci. Eng.* 2019; **577**, 012190.

[19] M Guo, J Jiang, Z Shen, Y Lin, CW Nan and Y Shen. High-energy-density ferroelectric polymer nanocomposites for capacitive energy storage: Enhanced breakdown strength and improved discharge efficiency. *Mater. Today* 2019; **29**, 49-67.

[20] M Tarnaoui, M Zaim, M Kerouad and A Zaim. First-principles effective Hamiltonian calculations of the electrocaloric effect in ferroelectric $Ba_xSr_{1-x}TiO_3$. *Phys. Lett. A* 2020; **384**, 126093.

[21] AS Everhardt, T Denneulin, A Grünebohm, YT Shao, P Ondrejkovic, S Zhou, N Domingo, G Catalan, J Hlinka, JM Zuo, S Matzen and B Noheda. Temperature-independent giant dielectric response in transitional $BaTiO_3$ thin films. *Appl. Phys. Rev.* 2020; **7**, 011402.

[22] H Wang, P Gopal, S Picozzi, S Curtarolo, MB Nardelli and J Sławińska. Spin hall effect in prototype Rashba ferroelectrics GeTe and SnTe. *npj Comput. Mater.* 2020; **6**, 7.

[23] VK Veerapandiyan, M Deluca, ST Misture,WA Schulze, SM Pilgrim and SC Tidrow. Dielectric and structural studies of ferroelectric phase evolution in dipole-pair substituted barium titanate ceramics. *J. Am. Ceram. Soc.* 2020; **103**, 287-96.

[24] YH Huang, YJ Wu, J Li, B Liu and XM Chen. Enhanced energy storage properties of barium strontium titanate ceramics prepared by sol-gel method and spark plasma sintering. *J. Alloys Compd.* 2017; **701**, 439-46.

[25] Z Zhao, X Liang, T Zhang, K Hu, S Li and Y Zhang. Effects of cerium doping on dielectric properties and defect mechanism of barium strontium titanate glass-ceramics. *J. Eur. Ceram. Soc.* 2020; **40**, 712-9 .

[26] C Gautam, A Madheshiya, AK Singh, KK Dey and M. Ghosh. Synthesis, optical and solid NMR studies of strontium titanate borosilicate glasses doped with TeO_2. *Results Phys.* 2020; **16**, 102914.

[27] Z Saroukhani, N Tahmasebi, SM Mahdavi and A Nemati. Effect of working pressure and annealing temperature on microstructure and surface chemical composition of barium strontium titanate films grown by pulsed laser deposition. *Bull. Mater. Sci.* 2015; **38**, 1645-50.

[28] R Manogowri, RM Mathelane, S Valanarasu, I Kulandaisamy, AB Fathima and A Kathalingam. Effect of annealing temperature on the structural, morphological, optical and electrical properties of Co_3O_4 thin film by nebulizer spray pyrolysis technique. *J. Mater. Sci. Mater. Electron.* 2016; **27**, 3860-6.

[29] HF Zhang, X Chen, J Gao, KM Lam, SD Liang, LF Fei, CL Mak and JF Chen. The fabrication and electrocaloric effect of bimodal-grain structure $(Ba_{0.60}Sr_{0.40})TiO_3$ using the induced abnormal grain growth method. *IOP Conf. Ser. Mater. Sci. Eng.* 2019; **678**, 012138.
[30] W Wang, M Zhang, L Xin, S Shen and J Zhai. Effect of interface behavior on dielectric properties of ferroelectric-dielectric composite ceramics. *J. Alloys Comp.* 2019; **809**, 151712.
[31] X Chen, S Im, J Kim and W Kim. Synthesis of barium-strontium titanate hollow tubes using Kirkendall effect. *J. Cryst. Growth*. 2018; **483**, 102-9.
[32] KH Lee, WH Shin, HS Kim, K Lee, JW Roh, J Yoo, J Kim, SW Kim and S Kim. Synergetic effect of grain size reduction on electronic and thermal transport properties by selectively-suppressed minority carrier mobility and enhanced boundary scattering in $Bi0.5Sb_{1.5}Te_3$ alloys. *Scripta Mater.* 2019; **160**, 15-9.
[33] S Pandey, O Parkash and D Kumar. Structural, dielectric, ferroelectric and impedance spectroscopic studies on $Ba_{1-x}Sr_xTiO_3$ ($0.15 \leq x \geq 0{:}35$). *Mod. Phys. Lett. B* 2019; **33**, 1950193.
[34] Y Zhai, X Xie, R Zhou, X Li, X Liu and S Liu. High performance room temperature ferroelectric barium strontium titanate ceramics by spark-plasma-sintering ultrafine nanocrystals. *Ceram. Int.* 2019; **45**, 15526-31.